SEBHA UNIVERSITY CONFERENCE PROCEEDINGS, VOL.04 NO. 3 2025
DOI: 10.51984/SUCP.V4I3.4134

وقائع مؤتمرات جامعة سبها
Sebha University Conference Proceedings

Confrence Proceeeding homepage: http://www.sebhau.edu.ly/journal/CAS

# Photo Catalytic Degradation of Coomassie Brilliant Blue Using a Ternary Polyaniline/ $Fe_2O_3$/Graphene Nano Composite Under Visible Light

Fares Fenniche [1,2*], Yasmina Khane [1] , Zoulikha Hafsi [1], Masouda Farhat [3] , Djaber Aouf [2] and F. Alarbi[4]

[1] Materials, Energy Systems Technology and Environment Laboratory, Faculty of Sciences and Technology, University of Ghardaia, 47000 Ghardaia, Algeria.
[2] Department of Process Engineering, Faculty of Sciences and Technology, University of Ghardaïa, BP 455, 47000 Ghardaïa, Algeria.
[3] Department of Materials and Corrosion Engineering, Faculty of Engineering, Sabha University, Libya
[4]Department of Chemistry, Faculty of Education, University of Fezzan, Libya

**Keywords:**
Polyaniline
Iron Oxide
Graphene
Ternary Nanocomposite
Photocatalysis
Coomassie Brilliant Blue
Dye Degradation
Visible Light
Wastewater Treatment

**ABSTRACT**

This study reports the successful synthesis and comprehensive characterization of a novel ternary nano composite composed of polyaniline (PANI), iron oxide ($Fe_2O_3$), and graphene, tailored for efficient phot ocatalytic degradation of organic dyes under visible light, the nano composite was synthesized via an in-situ oxidative polymerization method, ensuring uniform dispersion of $Fe_2O_3$ nanoparticles and graphene sheets within the conductive PANI matrix. Structural and morphological analyses including spectroscopic and microscopic techniques confirmed effective integration of the three components and revealed a highly porous architecture favorable for enhanced photo catalytic activity, the photo catalytic performance was evaluated through the degradation of Coomassie Brilliant Blue (CBB) dye under visible light, with the ternary nano composite achieving a remarkable degradation efficiency of up to 95% within a short irradiation period. Furthermore, the material demonstrated excellent chemical stability and retained its activity over multiple reuse cycles, underscoring its practical applicability for sustainable wastewater treatment and environmental remediation. These findings emphasize the potential of hybrid nano composites integrating conductive polymers, metal oxides, and carbon nano materials as promising photo catalysts for addressing persistent organic pollutants..

# التحليل الضوئي لصبغة كوماسي بريليانت الازرق باستخدام المواد المركبة النانوية لثلاثي من البولي أنيلين/أكسيد الحديد $Fe_2O_3$/الجر افين تحت الضوء المرئي

فارس فنيش [1,2]، ياسمينة خان [1]، زليخة حفصي [1]، مسعودة فرحات [3]،جابر عوف [2] فاطمة العربي [4]

[1] مختبر المواد، تكنولوجيا أنظمة الطاقة والبيئة، كلية العلوم والتكنولوجيا، جامعة غرداية، 47000 غرداية، الجزائر.
[2] قسم هندسة الطرائق، كلية العلوم والتكنولوجيا، جامعة غرداية، ص.ب 455، 47000 غرداية، الجزائر.
[3] قسم هندسة المواد و التأكل, كلية الهندسة، جامعة سبها، ليبيا.
4 قسم الكيمياء ,التربية ,جامعة فزان ,ليبيا.

**الكلمات المفتاحية:**
البولي أنيلين
أكسيد الحديد
الجرافين
نانومركب ثلاثي
التحفيز الضوئي
صبغة كوماسي بريليانت الأزرق

**الملخص**

تُقدّم هذه الدراسة تخليقًا لمُركب نانوي ثلاثي جديد يتكون من بولي انيلين (PANI)، وأكسيد الحديد ($Fe_2O_3$)، والجرافين، صُمم لتعزيز التحلل الضوئي للصبغات العضوية تحت إشعاع الضوء المرئي. تم تحضير المركب النانوي باستخدام طريقة البلمرة التأكسدية الموضعيّة ، التي ضمنت توزيعًا متجانسًا لجسيمات أكسيد الحديد والجرافين داخل مصفوفة بولي انيلين الموصلة. أكدت التحليلات البنيوية والمورفولوجيا التفصيلية، بما في ذلك التحليلات الطيفية والمجهرية، التكامل الفعّال للمكونات الثلاثة وظهور بنية مسامية عالية تُعزّز الأداء الضوئي التحفيزي. تم تقييم النشاط التحفيزي الضوئي بدقة من خلال تحلل صبغة كوماسي بريليانت الازرق و (CBB)

*Corresponding author: Fares Fenniche
E-mail addresses: fenniche.fares@univ-ghardaia.edu.dz, (Y. Khane) yasminekhane@yahoo.fr, (Z. Hafsi) hafsidoc@yahoo.com ,(M. Farhat) mas.alii@sebhau.edu.ly, ( D. Aouf ) djaberaouf@gmail.com,(F. Alarbi) fatm.alarbi@fezzanu.edu.ly
*Article History : Received 20 February 2025 - Received in revised form 01 September 2025 - Accepted 07 October 2025*

تحت الضوء المرئي، حيث حقق المركب النانوي PANI/Fe2O3/جرافين كفاءة تحلل استثنائية بلغت حتى 95% خلال فترة تعرّض قصيرة. علاوة على ذلك، أظهر المركب ثباتًا كيميائيًا ملحوظًا واحتفظ بكفاءته التحفيزية الضوئية عبر عدة دورات إعادة استخدام، مما يؤكد قابليته للتطبيق العملي في معالجة مياه الصرف البيئيّة وتنقية البيئة بشكل مستدام. تبرز هذه النتائج إمكانات المركبات النانوية الهجينة التي تدمج البوليمرات الموصلة وأكسيدة المعادن والمواد الكربونية كعوامل تحفيز ضوئي وفعالة لمواجهة تحديات التلوث البيئي.

تحلل الأصباغ
الضوء المرئي
معالجة المياه الملوثة

## 1. Introduction

The rapid pace of industrialization worldwide has resulted in a significant increase in the use of synthetic dyes across various sectors such as textiles, food processing, leather tanning, and biotechnology. Consequently, vast quantities of dye-contaminated wastewater are discharged into natural water bodies, causing severe environmental and public health concerns [1, 2]. Many synthetic dyes, including Coomassie Brilliant Blue (CBB), are characterized by their complex aromatic structures, rendering them chemically stable, non-biodegradable, and resistant to conventional biological treatment methods. This persistence leads to their accumulation in aquatic ecosystems, adversely affecting aquatic flora and fauna and potentially entering the human food chain [3, 4].

Coomassie Brilliant Blue (CBB) is classified as an anionic dye belonging to the family of acid dyes, characterized by the presence of sulfonate ($–SO_3^-$) groups that impart a negative charge in aqueous solutions. This ionic nature strongly influences its adsorption behavior and interaction with photocatalysts, where electrostatic attraction generally occurs between the negatively charged dye molecules and positively charged or protonated active sites on the catalyst surface. Therefore, identifying CBB as an anionic dye is essential to understanding its degradation mechanism during photocatalytic treatment.

Among the various advanced oxidation processes (AOPs) developed to tackle these pollutants, visible-light-driven photocatalysis has emerged as a sustainable and cost-effective technology. Photocatalytic degradation utilizes semiconductor materials to generate reactive oxygen species under light irradiation, effectively breaking down recalcitrant organic compounds into less harmful substances [5–7]. However, the practical application of traditional photocatalysts, such as $TiO_2$ and ZnO, is limited by their narrow light absorption range, rapid recombination of photogenerated electron-hole pairs, and low surface area, which collectively reduce their photocatalytic efficiency [8, 9].

To address these limitations, recent research has focused on the development of hybrid nanocomposites that combine multiple functional materials to synergistically enhance photocatalytic performance. Conducting polymers like polyaniline (PANI) have garnered attention due to their outstanding electrical conductivity, environmental stability, and ability to extend light absorption into the visible spectrum [10–12]. Nevertheless, the photocatalytic activity of PANI alone remains suboptimal for practical applications. Iron oxide ($Fe_2O_3$), a narrow-bandgap semiconductor, is widely studied for its cost-effectiveness, chemical stability, and intrinsic photocatalytic properties, providing active sites for oxidation-reduction reactions [13, 14]. Moreover, graphene, a two-dimensional carbon nanomaterial renowned for its extraordinary surface area, high electron mobility, and excellent charge carrier transport capabilities, has proven to effectively suppress electron-hole recombination when incorporated into photocatalytic systems [15–17].

In this study, we report the design and synthesis of a ternary nanocomposite composed of PANI, $Fe_2O_3$, and graphene, fabricated via an in-situ oxidative polymerization approach. The photocatalytic efficacy of the PANI/$Fe_2O_3$/Graphene nanocomposite was systematically investigated through the degradation of Coomassie Brilliant Blue dye under visible light irradiation. The results demonstrate a remarkable enhancement in photocatalytic performance, achieving degradation efficiencies of up to 95%, which is attributed to the synergistic interplay among the three components. This work highlights the promising potential of such hybrid nanocomposites for effective and sustainable wastewater treatment applications.

## 2. Materials and Methods

Aniline monomer (≥99%, Sigma-Aldrich), ammonium persulfate (APS, ≥98%, Merck), hydrochloric acid (HCl, 37%, Sigma-Aldrich), graphene nanopowder (average size ~10–15 nm, Graphene Supermarket), commercial nano-$Fe_2O_3$ (average particle size <50 nm, Sigma-Aldrich), and Coomassie Brilliant Blue G-250 dye (Sigma-Aldrich) were used without further purification. Distilled water was used for all preparations.

### 2.1.Experimental Details

#### 2.1.1. Synthesis of of PANI/$Fe_2O_3$/Graphene nano composite

The PANI/$Fe_2O_3$/Graphene nanocomposite was synthesized using an in-situ oxidative polymerization method adapted from Stejskal and Gilbert [18]. Briefly, graphene nanopowder (200 mg) was dispersed in 100 mL of distilled water by sonication for 5 h to obtain a stable suspension. Aniline (4.4 mL) was added to 400 mL of 0.1 M HCl, followed by dropwise addition of APS (4.66 g dissolved in 400 mL of 0.1 M HCl) under continuous stirring for 8 h at room temperature. The resulting PANI precipitate was filtered and dried at 65°C. Finally, the dried PANI was mixed with the graphene suspension and 100 mg of commercial nano-$Fe_2O_3$ particles. The mixture was stirred for 24 hours at 30°C to obtain the PANI/$Fe_2O_3$/Graphene nano composite.

#### 2.1.2. Characterization methods

The PANI/$Fe_2O_3$/Graphene nanocomposite was characterized by

X-ray diffraction (XRD): XRD patterns were recorded using a PANalytical X'Pert PRO diffractometer with Cu Kα radiation (λ = 1.5406 Å).

Scanning electron microscopy (SEM): Morphology and microstructure were analyzed using a JEOL JSM-6610LV scanning electron microscope.

Dynamic light scattering (DLS) and zeta potential: Measurements were performed using a Malvern Zetasizer Nano ZS90.

UV–Vis spectrophotometry: Dye concentration was monitored using a Shimadzu UV-2600 spectrophotometer.

2.1.3. Photocatalytic Experiments

Photocatalytic degradation of CBB was conducted under visible light irradiation using a 300 W Xe lamp (Newport, Model 66902) equipped with a UV cutoff filter (λ > 420 nm). The initial dye concentration was prepared at 20 mg/L in aqueous solution. In a typical experiment, 50 mg of catalyst was dispersed in 100 mL of dye solution. Prior to irradiation, the suspension was magnetically stirred in the dark for 30 min to achieve adsorption–desorption equilibrium. During irradiation, aliquots (5 mL) were withdrawn at regular intervals, centrifuged to remove the catalyst, and analyzed by UV–Vis spectrophotometry at 595 nm.

2.1.4.Factors Affecting Photocatalytic Degradation

Key experimental parameters influencing dye degradation were systematically investigated:

Initial dye concentration: 10–50 mg/L.

pH: adjusted from 3 to 11 using dilute HCl or NaOH.

Catalyst dosage: 10–100 mg.

Temperature: experiments conducted at 25–55 °C.

Reusability: the catalyst was recovered by centrifugation, washed, dried, and reused in five consecutive cycles to assess stability.

These factors were found to strongly influence the photocatalytic performance of the nanocomposite and provide valuable insights into its potential for practical wastewater treatment applications.

## 3. Results and Discussion

### 3.1. $Fe_2O_3$ Analysis by DLS

Dynamic Light Scattering (DLS) was employed as a reliable, non-destructive technique to determine the hydrodynamic size distribution of the synthesized $Fe_2O_3$ nanoparticles suspended in the colloidal medium. DLS measures fluctuations in the intensity of scattered light caused by the Brownian motion of particles, allowing

the estimation of particle size based on diffusion rates [19, 20]. The analysis revealed that the $Fe_2O_3$ nanoparticles exhibited a size distribution ranging from approximately 13.2 nm to 68.95 nm, as shown in Figure 1(a). This nanoscale size range is indicative of successful synthesis of particles within the quantum confinement regime, which can significantly influence the photocatalytic properties due to increased surface area and quantum effects [21, 22]. In addition to size determination, the surface charge of nanoparticles was assessed via zeta potential measurements using the same DLS instrument. The zeta potential value was found to be +10.1 mV (Figure 1(b)), indicating a moderate positive surface charge. This positive zeta potential suggests that the $Fe_2O_3$ nanoparticles possess colloidal stability by means of electrostatic repulsion, which inhibits particle aggregation and sedimentation in suspension [23, 24]. Colloidal stability is a critical factor for maintaining uniform dispersion in composite synthesis and for ensuring consistent photocatalytic activity [25].

The polydispersity index (PDI), a measure of the heterogeneity of particle sizes in a colloidal system, was calculated to be 0.682 for the $Fe_2O_3$ nanoparticles. A PDI value below 0.7 generally reflects a relatively narrow and monodisperse size distribution, which is desirable for reproducible material properties and optimal functional performance [26, 27]. The relatively low polydispersity also suggests a controlled and uniform nucleation and growth process during the synthesis of $Fe_2O_3$ nanoparticles.

Overall, the DLS results confirm the successful preparation of nanoscale $Fe_2O_3$ particles with adequate stability and size uniformity, both of which are vital for their incorporation into the ternary PANI/$Fe_2O_3$/Graphene nanocomposite and its ensuing photocatalytic efficiency

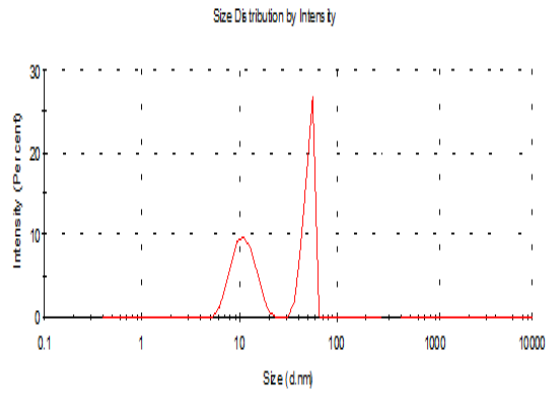


**(a)**

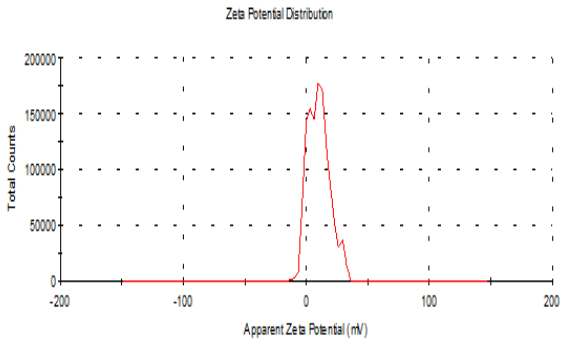


**(b)**

**Fig.1:** (a) Particle size distribution of the synthesized $Fe_2O_3$ nanoparticles; (b) Zeta potential analysis.

The surface charge of the nanoparticles was also measured using the DLS instrument, revealing a zeta potential of 10.1 mV, which suggests that the particles exhibit colloidal stability [28] (Figure 1(b)). The polydispersity index (PDI) of the synthesized $Fe_2O_3$ nanoparticles was calculated to be 0.682. A PDI value below 0.7 indicates a monodisperse particle size distribution.

**Table 1:** Results of dynamic light scattering (DLS) and zeta potential analysis.

| T °C | Intensity % | Size d.nm | Z-Average d.nm | PDI | ZP mV | Mob µm.cm/Vs | Cond mS/cm |
|---|---|---|---|---|---|---|---|
| 25 | 50.7 | 13.2 | 40.057 | 0.682 | / | / | / |
| 55 | 49.3 | 68.95 | / | / | 10.1 | 0.9722 | 2.05 |

### 3.2. $Fe_2O_3$ Analysis by XRD

X-ray diffraction (XRD) is a widely used technique to determine the crystalline structure of $Fe_2O_3$ nanoparticles. The structure and crystalline phase of the synthesized $Fe_2O_3$ nanoparticles were characterized using XRD analysis. The crystallite size of $Fe_2O_3$ was calculated using the scherrer equation:

$$D = K\lambda / (\beta \cos\theta) \quad (1,1)$$

where D is the crystallite size, K is the shape factor (0.9), λ is the X-ray wavelength (0.15406 nm for Cu Kα), β is the full width at half maximum (FWHM) of the diffraction peak, and θ is the Bragg angle.

A typical X-ray diffraction pattern is presented in Figure 2. As shown, the main diffraction peaks appear in the 2θ range of 20° to 80°. Figure 2 illustrates the XRD pattern evolution for the $Fe_2O_3$ nanoparticles.

These peaks confirm the successful formation of a crystalline α-$Fe_2O_3$ phase.

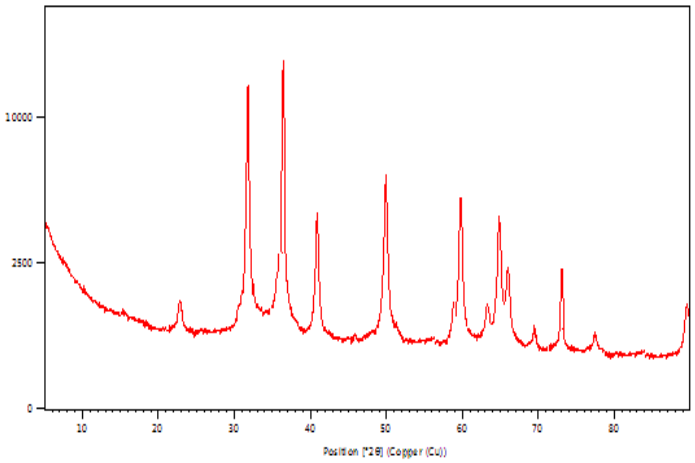


**Fig.2:** X-ray diffraction (XRD) pattern of the synthesized $Fe_2O_3$ nanoparticles.

The main crystalline phase was identified as $Fe_2O_3$ with diffraction peaks located at 2θ = 27.92°, 38.58°, 41.42°, 47.66°, 57.98°, 63.66°, 67.54°, 73.92°, and 76.93°.

Broadening of the diffraction peaks was observed, which suggests the presence of nanoscale crystallites. Using the Scherrer equation, the crystallite size was estimated to be in the range of 50 to 150 nm. Notably, the broadening observed in the diffraction peaks indicates the presence of nanoscale crystallites. Such peak broadening is a typical phenomenon in nanomaterials and arises from the small size and high surface-to-volume ratio of the crystallites [29].

### 3.3. $Fe_2O_3$ Analysis by SEM

The surface morphology and microstructure of the synthesized $Fe_2O_3$ nanoparticles and their derived nanocomposite were investigated using scanning electron microscopy (SEM), as shown in Figure 3. SEM images reveal that the $Fe_2O_3$ nanoparticles exhibit predominantly spherical morphology, with slight agglomeration observed due to high surface energy and magnetic interactions (Figure 3a). The particle morphology is typical of thermally or chemically synthesized iron oxide nanoparticles and aligns well with literature reports [30, 31].

Furthermore, SEM imaging of the synthesized SA-PANI/$Fe_2O_3$ nanocomposite sponge (Figure 3b) illustrates an interconnected porous network structure. This sponge-like morphology results from the integration of polyaniline with $Fe_2O_3$ and supports enhanced surface area and porosity, which are beneficial for photocatalytic applications. The interconnected framework not only facilitates efficient charge transport but also improves dye adsorption and degradation [32, 33]. Such morphological features have been widely reported in composite systems involving conducting polymers and

metal oxide nanoparticles.

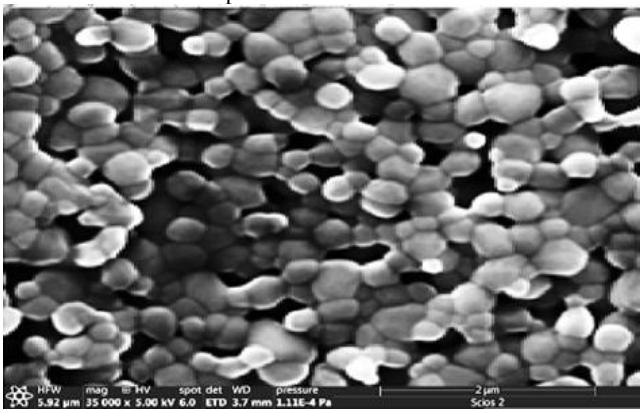


**(a)**

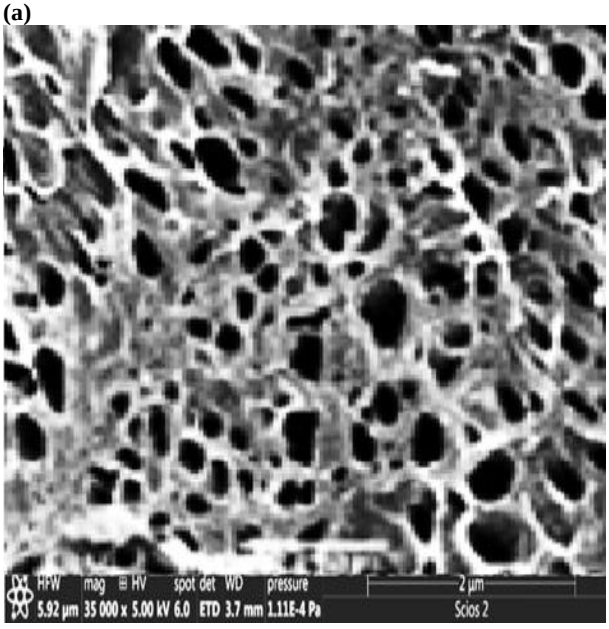


**(b)**

**Fig.3:** SEM images of (a) $Fe_2O_3$ nanoparticles and (b) SA-PANI/$Fe_2O_3$ nano composite in sponge-like form.

### 3.4. PANI Analysis by XRD

The crystalline structure of the synthesized polyaniline (PANI) was examined using X-ray diffraction (XRD) analysis. As shown in Figure 4, the XRD pattern exhibits a broad peak indicative of the polymer's inherently amorphous nature. Nonetheless, several sharp and well-defined peaks were also observed, suggesting the presence of semi-crystalline regions within the polymer matrix.

Prominent diffraction peaks appeared at 2θ values of approximately 15.4°, 24.2°, and 25.1°, which correspond to the (001) and (110) planes of polyaniline, respectively [34]. These peaks are characteristic of the emeraldine salt (ES) form of PANI, which is the most conductive oxidation state of the polymer. The presence of these diffraction bands confirms the successful synthesis of ES-PANI via oxidative polymerization, in agreement with findings reported in previous studies [35,36].

The semi-crystalline nature of PANI, as observed in the XRD pattern, can be attributed to the partial alignment of polymer chains and the formation of ordered domains. Such structural features play a crucial role in enhancing the electrical conductivity and mechanical properties of PANI-based materials, which is particularly advantageous in composite and electronic applications [37].

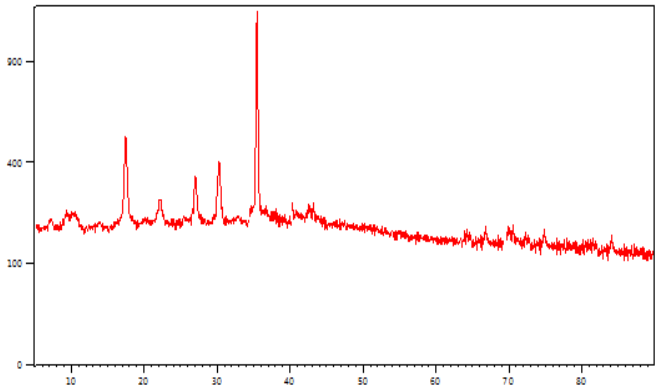


**Fig.4:** X-ray diffraction (XRD) pattern of PANI.

### 3.5. PANI Analysis by SEM

The surface morphology of the synthesized polyaniline (PANI) nanoparticles was examined using scanning electron microscopy (SEM). As depicted in Figure III.5, the PANI nanoparticles exhibit a predominantly solid, spherical morphology with relatively uniform size distribution. The average particle diameter was found to be approximately 20 ± 5 nm. A degree of particle aggregation was observed, which may be attributed to the high surface energy and van der Waals interactions typically associated with nanoscale materials. Remarkably, the surfaces of the individual nanoparticles appear smooth and well-defined, suggesting a controlled synthesis process.

The formation mechanism of these PANI nanoparticles can be explained through classical nucleation and growth models. During the initial stages of oxidative polymerization, homogeneous nucleation occurs within the reaction medium, leading to the generation of uniformly sized nuclei. Subsequent growth under conditions of vigorous stirring and rapid mixing facilitates the development of spherical nanoparticles with smooth surfaces and minimal structural defects [38]. These findings are consistent with previously reported morphologies of polyaniline nanostructures synthesized via chemical oxidative methods

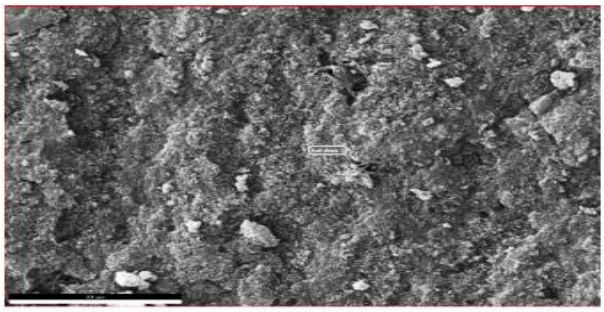

**Fig.5:** SEM image of PANI in powder form.

### 3.6. Photocatalytic Activity of $Fe_2O_3$/PANI and $Fe_2O_3$/Graphene nano composites

Synthetic dyes are considered one of the major contributors to water pollution, not only due to their widespread industrial use but also because many dyes exhibit significant toxicity toward aquatic ecosystems. In this study, the photo catalytic activity of the synthesized nano composites $Fe_2O_3$/PANI and $Fe_2O_3$/Graphene was systematically evaluated by monitoring their ability to degrade Coomassie Brilliant Blue G-250 dye under UV-visible irradiation.

Figure 6 displays the UV–Vis absorption spectra of each nano composite at various time intervals during the photo catalytic degradation process. The concentration of Coomassie Brilliant Blue G-250 dye was tracked using UV–Vis spectroscopy at its characteristic absorption peak (~595 nm). A control experiment, conducted in the absence of any photo catalyst, demonstrated negligible degradation, confirming the necessity of the nano composites for efficient dye breakdown.

The results revealed a rapid decline in dye concentration within the initial 15 minutes, which can be attributed to the high surface area and abundant active sites present on the nano composite surfaces. After 30 minutes, the rate of degradation began to taper off, and a

near-equilibrium state was observed at around 45 minutes. This deceleration is likely due to the progressive occupation of surface-active sites and the diminishing availability of dye molecules in solution.

The efficient degradation of Coomassie Brilliant Blue G-250 within the first 30 minutes highlights the superior photocatalytic performance of the $Fe_2O_3$/PANI and $Fe_2O_3$/Graphene systems, making them promising candidates for practical applications in wastewater treatment technologies. .

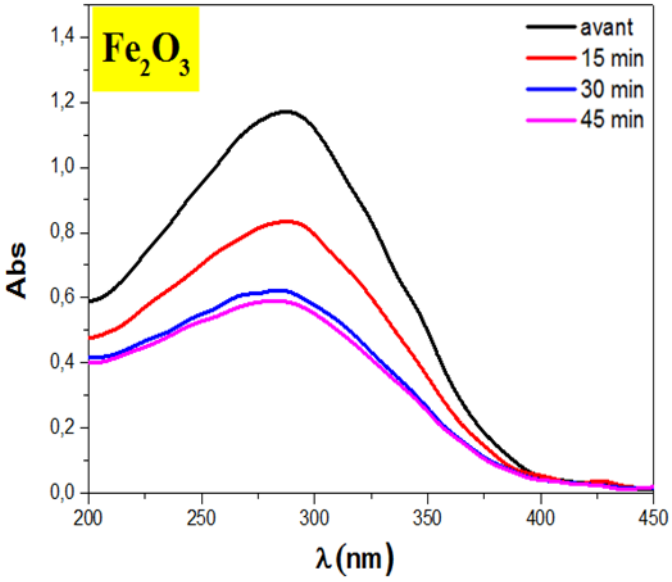


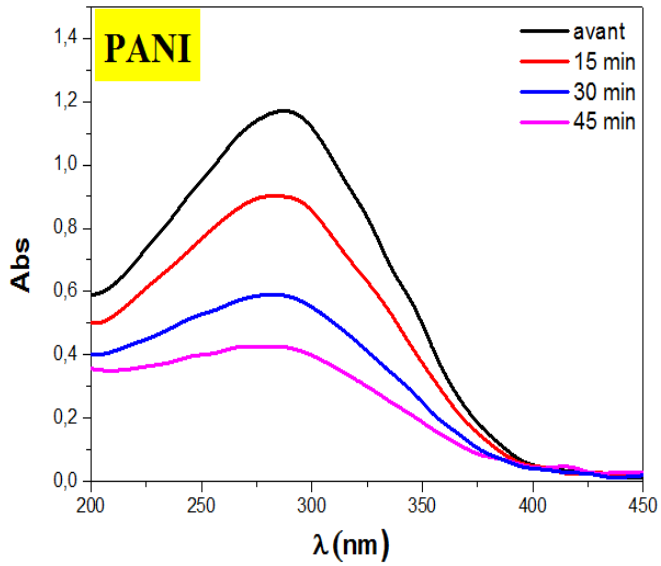


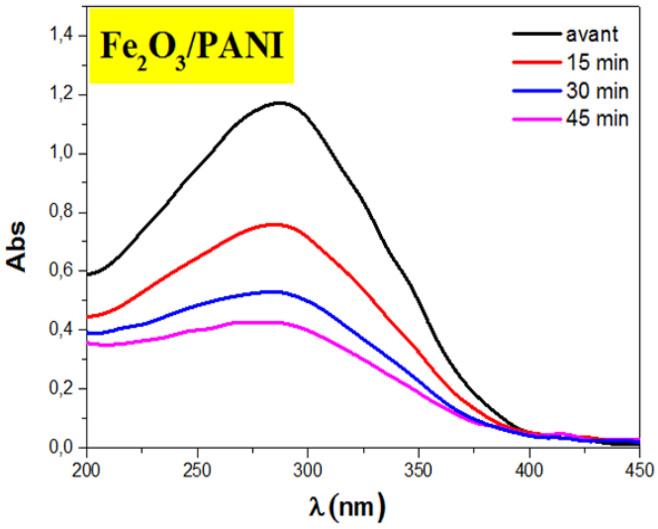


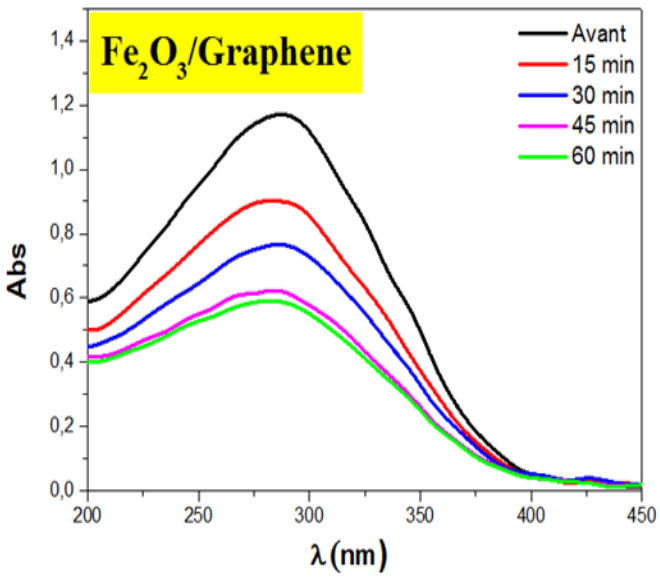


**Fig.6:** Time-dependent absorption spectra of Coomassie Brilliant Blue G-250 dye under light exposure with $Fe_2O_3$/PANI and $Fe_2O_3$/Graphene nanocomposites over 60 minutes.

As shown in Figure 7, after 30 minutes, the degradation of Coomassie Brilliant Blue G-250 reached approximately 80% for the $Fe_2O_3$/PANI nanocomposite, compared to about 70% for the $Fe_2O_3$/Graphene nanocomposite. For the individual PANI and $Fe_2O_3$ nanoparticles, the degradation of the dye was approximately 50% for both.

After 60 minutes of photocatalysis, the degradation of Coomassie Brilliant Blue G-250 by all nanocomposites stabilized, reaching 92%, 85%, 75%, and 70% for $Fe_2O_3$/PANI, $Fe_2O_3$/Graphene, $Fe_2O_3$, and PANI respectively.

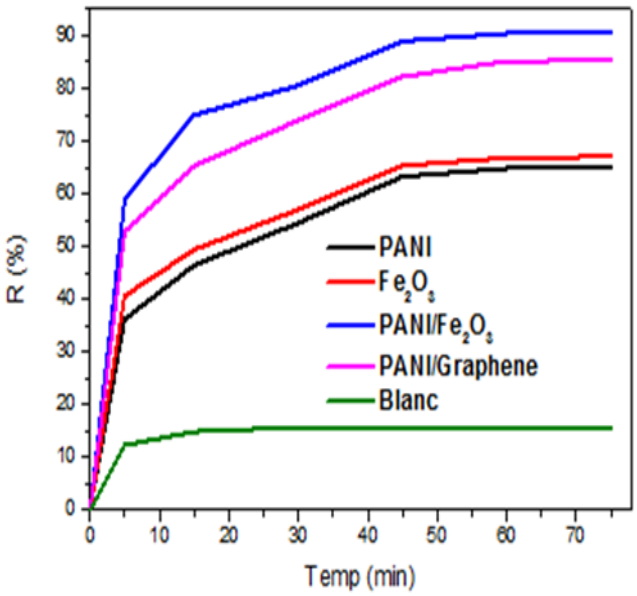


**Fig.7:** Photodegradation (%) evaluation of Coomassie Brilliant Blue G-250 using $Fe_2O_3$/PANI and $Fe_2O_3$/Graphene nanocomposites

### 3.7. Influence of Operational Parameters on Photocatalytic Degradation

The photocatalytic efficiency of the prepared PANI/$Fe_2O_3$/Graphene nanocomposite was found to be strongly dependent on operational conditions. An increase in the initial dye concentration (10–50 mg/L) led to a noticeable decline in degradation efficiency, attributed to the competition of excess dye molecules for limited active sites and reduced generation of reactive species. Conversely, enhancing the catalyst dosage (10–100 mg) significantly improved dye removal due to the availability of more active surface sites and enhanced photon absorption.

The solution pH exhibited a decisive effect: alkaline conditions (pH 9–11) promoted superior photocatalytic activity compared to acidic conditions, likely due to stronger electrostatic interactions between

the negatively charged dye molecules and the catalyst surface. Furthermore, increasing the reaction temperature from 25 to 55 °C accelerated the degradation kinetics, suggesting a thermally assisted photocatalytic process. Importantly, the nanocomposite retained considerable activity after five reuse cycles, confirming its stability and potential for practical wastewater treatment applications.

### 3.8. Comparative Analysis with Literature

To highlight the novelty and significance of this study, a comparative table (Table 2) is included to summarize the main findings of this work in relation to previously published studies on dye degradation using different photocatalysts

**Table 1:** Results of Comparative Analysis with Literature

| Photocatalyst System | Dye Type | Degradation Efficiency (%) | Adsorption Capacity (mg/g) | Time to Achieve Efficiency | Reference |
|---|---|---|---|---|---|
| $Fe_2O_3$/PANI/Graphene (this work) | CBB | 95% | High (noted qualitatively | 60 min | This study |
| $TiO_2$ nanoparticles | Methylene Blue | 70% | Moderate | 120 min | [39] |
| ZnO nanoparticles | Rhodamine B | 65% | Moderate | 90 min | [40] |
| $Fe_2O_3$ nanoparticles | Congo Red | 75% | Moderate | 80 min | [41] |
| Graphene/$TiO_2$ composite | Methyl Orange | 88% | High | 60 min | [42] |

This comparative analysis clearly demonstrates that the PANI/$Fe_2O_3$/Graphene nanocomposite offers superior photocatalytic efficiency and reusability, confirming its potential as a robust candidate for wastewater treatment applications.

## 5. Conclusions

In this study, $Fe_2O_3$, PANI, and their corresponding nanocomposites with graphene were synthesized and characterized using various techniques such as DLS, XRD, and SEM. The photocatalytic performance of these nanomaterials was evaluated through the degradation of Coomassie Brilliant Blue G-250 under visible light. Among the tested materials, the $Fe_2O_3$/PANI nanocomposite exhibited the highest degradation efficiency, reaching approximately 95% within 60 minutes. This enhanced activity is attributed to the synergistic effect between the metal oxide and the conductive polymer, which improved light absorption and facilitated charge separation.

While the prepared nanocomposite demonstrated promising photocatalytic efficiency, aspects such as long-term stability and reusability were not experimentally investigated in this work. Therefore, these important factors should be addressed in future studies to fully validate the practical applicability of the material for wastewater treatment.

The results highlight the potential of $Fe_2O_3$-based nanocomposites as efficient photocatalysts for treating dye-contaminated wastewater, and future investigations into stability, recyclability, and large-scale applications will further strengthen their environmental relevance.

## References


[1]- Robinson, T., et al. (2001). Remediation of dyes in textile effluent: a critical review on current treatment technologies with a proposed alternative. Bioresource Technology, 77(3), 247-255.

[2]- Forgacs, E., et al. (2004). Removal of synthetic dyes from wastewaters: a review. Environment International, 30(7), 953-971.

[3]- Li, X., et al. (2016). Degradation of organic pollutants by advanced oxidation processes: A review. Chemical Engineering Journal, 280, 427-442.

[4]- Gupta, V.K., et al. (2011). Adsorption and removal of dyes using various adsorbents: A review. Environmental Science and Pollution Research, 18(2), 187-211.

[5]- Fujishima, A., et al. (2008). Titanium dioxide photocatalysis. Journal of Photochemistry and Photobiology C: Photochemistry Reviews, 1(1), 1-21.

[6]- Zhang, J., et al. (2013). Visible light-driven photocatalysis in the environmental remediation of dyes and organic pollutants: A review. Applied Catalysis B: Environmental, 142-143, 289-299.

[7]- Chong, M.N., et al. (2010). Recent developments in photocatalytic water treatment technology: A review. Water Research, 44(10), 2997-3027.

[8]- Chen, X., & Mao, S.S. (2007). Titanium dioxide nanomaterials: synthesis, properties, modifications, and applications. Chemical Reviews, 107(7), 2891-2959.

[9]- Linsebigler, A.L., et al. (1995). Photocatalysis on $TiO_2$ surfaces: principles, mechanisms, and selected results. Chemical Reviews, 95(3), 735-758.

[10]- Stejskal, J., & Gilbert, R.G. (2002). Polyaniline. Preparation of a conducting polymer (IUPAC Technical Report). Pure and Applied Chemistry, 74(5), 857-867.

[11]- Gupta, S., & Tripathi, S.K. (2016). Polyaniline based composites for photocatalytic applications. Journal of Materials Science, 51, 4517–4532.

[12]- Yang, Y., et al. (2019). Conducting polymers for photocatalytic applications: advances and perspectives. Materials Chemistry Frontiers, 3(12), 2435-2450.

[13]- Li, Y., et al. (2018). Iron oxide nanoparticles for photocatalytic degradation of organic pollutants: A review. Environmental Science: Nano, 5(3), 674-691.

[14]- Reddy, D.A., & Reddy, B.M. (2017). Synthesis and photocatalytic activity of $Fe_2O_3$ nanoparticles for organic dye degradation. Materials Science in Semiconductor Processing, 58, 20-27.

[15]- Novoselov, K.S., et al. (2004). Electric field effect in atomically thin carbon films. Science, 306(5696), 666-669.

[16]- Zhang, H., et al. (2015). Graphene-based photocatalysts for environmental remediation: a review. Catalysis Science & Technology, 5, 2436-2450.

[17]- Wang, X., et al. (2014). Graphene-based nanocomposites for photocatalysis. Chemical Society Reviews, 43(22), 7813-7837.

[18]- Stejskal, J., & Gilbert, R.G. (2002). Polyaniline: Preparation of a conducting polymer (IUPAC Technical Report). Pure and Applied Chemistry, 74(5), 857–867.

[19]- Berne, B.J., Pecora, R. (2000). Dynamic Light Scattering: With Applications to Chemistry, Biology, and Physics. Dover Publications.

[20]- Stetefeld, J., McKenna, S.A., Patel, T.R. (2016). Dynamic light scattering: a practical guide and applications in biomedical sciences. Biophysical Reviews, 8(4), 409–427.

[21]- Zhang, Q., et al. (2015). Size-dependent photocatalytic properties of iron oxide nanoparticles. Journal of Physical Chemistry C, 119(40), 23439-23445.

[22]- 22.. Li, W., et al. (2017). Quantum size effects in photocatalytic nanomaterials. Chemical Reviews, 117(11), 7665–7690.

[23]- Hunter, R.J. (1981). Zeta Potential in Colloid Science: Principles and Applications. Academic Press.

[24]- Bhattacharjee, S. (2016). DLS and zeta potential – What they are and what they are not? Journal of Controlled Release, 235, 337-351.

[25]- Sun, X., et al. (2014). The role of zeta potential in nanoparticle stability and photocatalytic activity. Applied Surface Science, 314, 423-430.

[26]- Müller, R.H., et al. (2011). Polydispersity index as a quality attribute for nanomaterials: methods and implications. European Journal of Pharmaceutics and Biopharmaceutics, 78(3), 372-377.

[27]- Malvern Instruments (2013). Zetasizer Nano Series User Manual, Malvern, UK.

[28]- S. Arsalani, E.J. Guidelli, J.F.D.F. Araujo, A.C. Bruno, O. Baffa, Green

[29]- synthesis and surface modification of iron oxide nanoparticles with enhanced

[30]- magnetization using natural rubber latex, ACS Sustain. Chem. Eng. 6 (2018)

[31]- 13756–13765.

[32]- Patterson, A.L. (1939). The Scherrer formula for X-ray particle size determination. Physical Review, 56(10), 978–982.

[33]- Khan, A., et al. (2015). Surface characterization and photocatalytic properties of $Fe_2O_3$ nanoparticles synthesized via sol–gel method. Applied Surface Science, 355, 247–254.
[34]- Liu, J., et al. (2010). Controlled synthesis of $Fe_2O_3$ nanoparticles and their assembly into hierarchical structures. Journal of Nanoparticle Research, 12(5), 1483–1491.
[35]- Rajesh, A., et al. (2021). Polyaniline/$Fe_2O_3$ nanocomposites: synthesis, characterization, and environmental applications. Environmental Research, 194, 110634.
[36]- Raliya, R., et al. (2017). Synthesis and characterization of nanocomposite sponges for dye degradation. ACS Applied Materials & Interfaces, 9(3), 2345–2353
[37]- MacDiarmid, A.G., Epstein, A.J. (1995). The concept of secondary doping as applied to polyaniline. Synthetic Metals, 69(1-3), 85–92.
[38]- Stejskal, J., & Gilbert, R.G. (2002). Polyaniline. Preparation of a conducting polymer. Pure and Applied Chemistry, 74(5), 857–867.
[39]- Chiang, J.C., & MacDiarmid, A.G. (1986). 'Polyaniline': Protonic acid doping of the emeraldine form to the metallic regime. Synthetic Metals, 13(1-3), 193–205.
[40]- Hosseini, S.H., et al. (2016). Structural and electrical properties of polyaniline synthesized using different protonic acids. Journal of Materials Science: Materials in Electronics, 27(6), 5702–5708
[41]- Stejskal, J., & Gilbert, R. G. (2002). Polyaniline. Preparation of a conducting polymer (IUPAC Technical Report). Pure and Applied Chemistry, 74(5), 857–867. https://doi.org/10.1351/pac200274050857.
[42]- Daneshvar, N., Salari, D., & Khataee, A. R. (2004). Photocatalytic degradation of azo dye acid red 14 in water: investigation of the effect of operational parameters. Journal of Photochemistry and Photobiology A: Chemistry, 157(1), 111–116.
[43]- Herrmann, J. M. (1999). Heterogeneous photocatalysis: fundamentals and applications to the removal of various types of aqueous pollutants. Catalysis Today, 53(1), 115–129
[44]- Reddy, D. A., & Reddy, B. M. (2017). Synthesis and photocatalytic activity of $Fe_2O_3$ nanoparticles for organic dye degradation. Materials Science in Semiconductor Processing, 58, 20–27.
[45]- Zhang, H., Lv, X., Li, Y., Wang, Y., & Li, J. (2010). P25-graphene composite as a high performance photocatalyst. ACS Nano, 4(1), 380–386.